Journal of Power Sources 201 (2012) 280–287

Contents lists available at SciVerse ScienceDirect

Journal of Power Sources

journal homepage: www.elsevier.com/locate/jpowsour

Design of composite polymer electrolytes for Li ion batteries based on mechanical stability criteria

Sergiy Kalnaus*, Adrian S. Sabau, Wyatt E. Tenhaeff, Nancy J. Dudney, Claus Daniel

Materials Science and Technology Division, Oak Ridge National Laboratory, Oak Ridge, TN 37831-6083, USA

ARTICLE INFO

Article history:
Received 29 August 2011
Received in revised form 6 November 2011
Accepted 7 November 2011
Available online 17 November 2011

Keywords:
Lithium ion battery
Composite electrolyte
Effective properties
Lithium anode
Dendrites

ABSTRACT

Mechanical properties and conductivity were computed for several composite polymer electrolyte structures. A multi-phase effective medium approach was used to estimate effective conductivity. The Mori–Tanaka approach was applied for calculating the effective stiffness tensor of the composites. An analysis of effective mechanical properties was performed in order to identify the composite structures, which would be capable of blocking the dendrites forming in Li-ion battery when Li metal is used as anode. The stability parameter which combines both stiffness and compressibility of the electrolyte was used in the analysis. The calculations were done over the wide range of Young's modulus of the polymer matrix showing the threshold concentration of the filler necessary for the mechanical stability. The results can be used to formulate design criteria for solid electrolytes that would exhibit appropriate stiffness and compressibility to suppress lithium dendrite growth while maintaining high effective conductivities.

1. Introduction

Lithium-ion batteries used in consumer and automotive applications are traditionally based on liquid electrolytes. Liquid electrolytes are both thermodynamically unstable and flammable, raising the concern for safety of lithium ion batteries. Utilization of solid electrolytes will eliminate the need of use of flammable solvents and will increase the safety of Li-ion batteries. In addition, if solid electrolytes possess appropriate mechanical properties, they would suppress the anode roughening and would prevent Li dendrite growth which may lead to shorting the battery. This property in turn will promote the use of metallic lithium as anode, which will increase the energy density of the battery. It was recently postulated, based on computational results for the stability of Li electrodes [1], that there is a threshold for the shear modulus above which the dendritic growth would be suppressed. The shear modulus threshold was found to decrease with the compressibility of the electrolyte, property that is quantified using Poisson's ratio, ν. For example, for $\nu = 0$ (fully compressible), 0.33, and 0.5 (incompressible), a material with corresponding shear modulus of approximately 4, 2, and 1 times that of the lithium metal would prevent the amplification of electrode roughness.

Invention of lithium phosphorus oxynitride (LiPON) solid electrolyte [2–5] for thin film battery application opened new perspectives in solid state Li-ion technology. LiPON has a typical composition as $Li_{3.3}PO_{3.8}N_{0.22}$, possesses good lithium conductivity of 2.3 $\mu S\,cm^{-1}$ [3,5], and is stable at high cell voltage. In addition, being a hard glassy material, LiPON is expected to suppress lithium anode roughening and dendrite protrusion. Unfortunately, LiPON would crack under the tensile stresses developed during the battery cycling as it is a brittle material.

In this study, composite electrolyte structures with conductive polymer matrix and LiPON reinforcement are sought to overcome this brittleness problem. Typical polymer matrix can be represented by a complex of lithium salt (LiX) with a high molecular weight polymer, typically PEO [6–9]. Such combination is promising in enhancing the overall mechanical properties while maintaining good ionic conductivity. Significant amount of experimental research conducted on polymer electrolytes shows that improvement in mechanical properties [10] and conductivity [6,10,11] can be achieved by means of addition of small particles to the polymer matrix. Experiments were conducted mostly with PEO-based electrolytes mixed with insulating particles of Al_2O_3 [6–8,11–17], TiO_2 [7,15,18], ZrO_2 [9], and SiO_2 [8,17]. In all of these cases, a substantial increase in the conductivity, compared to the conductivity of the polymer, was observed.

It was suggested that the main mechanism responsible for conductivity increase is the formation of a shell consisting of amorphous polymer around each particle [19–22]. Such explanation was based on the X-ray studies that revealed a decreased degree of crystallinity in samples with Al_2O_3 particles dispersed in a polymer matrix [23]. Similar results of decrease in polymer crystallinity and increased conductivity behavior were obtained from experiments on PEO mixtures with higher molecular weight polyacrylamide

* Corresponding author. Tel.: +1 865 576 6181; fax: +1 865 574 4357.
E-mail address: kalnauss@ornl.gov (S. Kalnaus).

0378-7753/$ – see front matter © 2011 Elsevier B.V. All rights reserved.
doi:10.1016/j.jpowsour.2011.11.020

Table 1
Conductivities (25 °C) of the three phases of CPE (S cm^{-1}).

LiPON [3,4]σ_f	(PEO)$LiClO_4$ [26]σ_m	Amorphous (PEO)$LiClO_4$ [26]σ_s
2.3×10^{-6}	8.1×10^{-8}	3.59×10^{-6}

(PAAM) [24–26]. It has to be mentioned that to the best of the author's knowledge there is no experimental evidence for the highly conductive amorphous polymer layer at the LiPON/Polymer interface. This is due to the fact that the investigation of LiPON as a candidate for composite polymer electrolyte (CPE) reinforcement has just emerged and the measurement of properties and/or phase characterization at microscale is ongoing.

In the optimized configuration, the CPE for Li ion battery with lithium anode would be structured in such a way that its mechanical properties are enhanced enough to prevent cracking as well as suppress dendrite penetration, while the conductivity is increased compared to the conductivity of the reinforcing phase. In the present investigation, an analysis of both conductivity and elastic properties is performed for the composite microstructures. The reinforcement medium is considered to be either spherical particles or flakes of a given thickness. The effective conductivity and effective stiffness tensor are estimated for different distributions of the filler phase. Composites with conductive reinforcement phase (prototyped after LiPON) are considered. General effective medium theory of McLachlan, which is here modified for a three-phase system, is applied for determination of effective composite conductivity. The Mori–Tanaka approach is used for estimating the effective mechanical properties of the material. In the mechanical analysis, the effect of the amorphous polymer phase, i.e., the highly conductive shell surrounding the filler components, on the mechanical properties of the CPE is negligible due to its very low stiffness as compared to that of the filler. Finally, several CPE electrolyte architectures for Li batteries are proposed based on the results from the numerical simulations of CPE properties.

2. Material properties

Material properties for the constituents of the composite electrolyte were available from several references. The conductivities of the three phases at 25 °C, which were obtained from the corresponding Arrhenius or VTF equations, are listed in Table 1 together with the corresponding references in which the equation parameters are reported. The subscripts *f*, *m* and *s* represent filler, matrix and shell phases of the composite, respectively. Conductivity of the shell is assumed to be equal to the conductivity of amorphous phase (PEO) $LiClO_4$.

Young's modulus and Poisson's ratio for LiPON were obtained from a recent nano-indentation study [27] where they are reported to be equal to 77 GPa and 0.25, respectively. Young's modulus of PEO was measured to be 0.2–5 GPa for thin films [28] and 0.29 GPa for highly crystalline bulk material [29]. The Poisson's ratio of PEO was 0.49 [29]. The high value (5 GPa) for the Young's modulus was obtained for thin films using large force indentation experiments [28] and may be relevant to the composites produced by pressing techniques. For PEO nanofibers, Bellan et al. report Young's modulus values between 0.5 and 7.0 GPa [30]. The chain Young's modulus of 13 GPa was determined from Raman measurements [31] and can serve as the upper limit of the elastic modulus.

Evaluation criteria for the mechanical properties of CPE block is based on the analysis performed by Monroe and Newman [1], in which it was postulated, based on linear stability analysis, that Li surface stability is achieved when the shear modulus of electrolyte would be greater than approximately twice the shear modulus of lithium metal when $\nu = 0.33$. This shear modulus threshold was found to decrease with Poisson's ratio. A lower Poisson's ratio – which indicates high compressibility, would require larger shear modulus for stability of the electrode surface. For incompressible electrolytes, i.e., $\nu \to 0.5$, the shear modulus threshold was estimated to be approximately half as that for $\nu = 0.33$, i.e., $G_{eff}/G_{Li} = 1.0$ while for fully compressible electrolytes, i.e., $\nu \to 0$, the shear modulus threshold was approximately twice as that for $\nu = 0.33$, i.e., $G_{eff}/G_{Li} = 4.0$. In this paper, G_{Li} and G_{eff} denote the shear modulus of lithium metal and effective shear modulus of the electrolyte respectively. Based on these reported findings [1], a stability parameter that is dependent of Poisson's ratio is introduced in this study by linear regression analysis of G_{eff}/G_{Li} corresponding to the threshold points when electrode stability is achieved. The values of G_{eff}/G_{Li} higher than the threshold are considered providing stability at Li metal surface and in this case the condition for stability parameter (ξ) is expressed as

$$\xi = (a_1 + a_2\nu)\frac{G_{Li}}{G_{eff}} \leq 1 \tag{1}$$

with fitting constants being: $a_1 = 3.503$; $a_2 = -5.034$. By means of Eq. (1) the influence of both effective shear modulus and Poisson's ratio is considered in one parameter which aids further analysis of the results.

3. Computational methodology

In this section, the computational methodology is presented for both the effective conductivity and the effective elastic properties of the CPE.

3.1. Effective conductivity

Schematics of the particulate CPE microstructure, which is considered for the effective conductivity calculations, are shown in Fig. 1. The two-dimensional cross section in Fig. 1 can be representative of a three-dimensional particulate composite. Three distinct phases, each possessing its own conductivity and playing role in overall performance of the electrolyte, can be identified in Fig. 1. Based on the conductivity property data of PEO-based electrolytes and LiPON (Table 1), the conductivity of the phases is ordered in increasing value as $\sigma_f < \sigma_m < \sigma_s$. Due to the lack of any experimental data regarding the dependence of the shell thickness on the particle size, the shell thickness was considered to be the same for all the reinforcing elements in the composite. Since the existence of the highly conductive amorphous polymer layer was not yet confirmed at the LiPON/Polymer interface, additional calculations were performed without considering the amorphous shell, i.e., $\sigma_s = \sigma_m$.

Several analytical formulations for the prediction of composite effective conductivity are widely available. The most known formulations are Brick-Layer Model (series and parallel), Maxwell Theory, McLachlan's Generalized EMT (GEMT), and others. Several representative EMT-type models are arranged in Table 2 [32–34]. These models were derived for two-phase mixtures. It has been shown that GEMT and Symmetric Bruggeman EMT (SBMT) models are accurate for two-phase particulate composites [32]. In this study, the GEMT is extended from two-phase to three-phase following the method suggested by Nan and Smith [22,34]. The series and parallel models are used to represent layered structures, which would be obtained with LiPON flakes running parallel or perpendicular to the electrode surface.

The two-phase models listed in Table 2 can be used directly to estimate effective conductivity for cases where the effect of interfacial shell layer between the particle and the matrix is neglected. In order to take into account the different conductivity of the shell these formulations need to be adjusted. This is typically done by lumping the filler and shell, i.e., as another filler with a

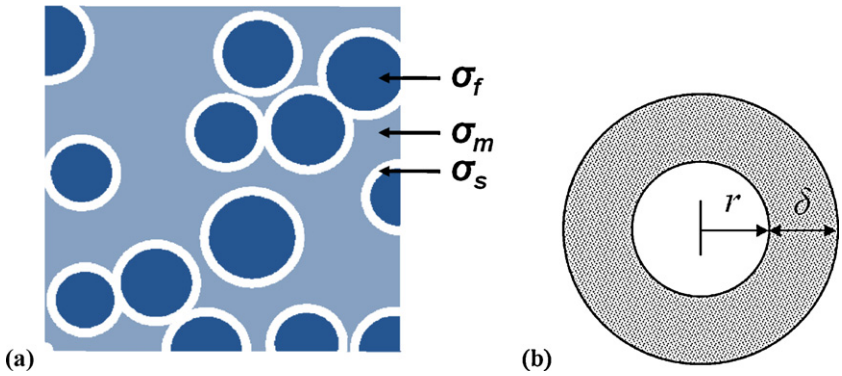

Fig. 1. Schematics of the 3-phase particulate CPE: (a) 2D representation of CPE structure and (b) composite particle consisting of filler particle of radius r and conductive shell of thickness δ.

conductivity computed from the conductivities of the original filler and shell [20–23]. For instance, in case of a spherical particle (Fig. 1b), the effective conductivity ($\tilde{\sigma}$) of a composite particle consisting of the filler particle and conductive shell can be expressed following the MWT approach ($d = 3$)

$$\frac{\tilde{\sigma} - \sigma_f}{\tilde{\sigma} + 2\sigma_f} = (1 - \tilde{g})\frac{\sigma_s - \sigma_f}{\sigma_s + 2\sigma_f} \tag{2}$$

where the volume fraction of the filler in the composite particle $\tilde{g}$ can be calculated as:

$$\tilde{g} = \frac{r^3}{(r+\delta)^3} = \frac{1}{(1+\alpha)^3} \tag{3}$$

where $\alpha = \delta/r$ is dimensionless shell thickness parameter. The volume fraction of the composite particles in matrix becomes $g/\tilde{g}$ and the GEMT effective conductivity equation for the composite electrolyte is modified accordingly, as:

$$\left(\frac{g}{\tilde{g}}\right)\frac{\tilde{\sigma}^{1/t_1} - (\sigma_{eff})^{1/t_1}}{\tilde{\sigma}^{1/t_1} + (1/g_e^{(1)} - 1)(\sigma_{eff})^{1/t_1}} + \left(1 - \frac{g}{\tilde{g}}\right)\frac{\tilde{\sigma}^{1/t_1} - (\sigma_{eff})^{1/t_1}}{\tilde{\sigma}^{1/t_1} + (1/g_e^{(1)} - 1)(\sigma_{eff})^{1/t_1}} = 0 \tag{4}$$

The conductivity of the three-phase system, which is shown in Fig. 1, has two percolation thresholds, $g_e^{(1)}$ and $g_e^{(2)}$, as has been shown experimentally [20–23]. Therefore the effective conductivity curve as a function of filler volume fraction has two distinct regions. In the first region, the conductivity increases due to increase in the fraction of the highly conductive shell. Equation 4 is valid in this region. When the material is saturated by the filler fraction at a point when $g = \tilde{g}$ ($g^* = \tilde{g}$), the microstructure is essentially represented by the shell and filler phases. Beyond this threshold point, the conductivity starts decreasing due to an increase in the volumetric fraction of the reinforcement phase, which has the lowest conductivity. In this regime Eq. (4) is written as

$$g\frac{\sigma_f^{1/t_2} - (\sigma_{eff})^{1/t_2}}{\sigma_f^{1/t_2} + (1/g_e^{(2)} - 1)(\sigma_{eff})^{1/t_2}} + (1-g)\frac{\sigma_s^{1/t_2} - (\sigma_{eff})^{1/t_2}}{\sigma_s^{1/t_2} + (1/g_e^{(2)} - 1)(\sigma_{eff})^{1/t_2}} = 0 \tag{5}$$

The results presented in Fig. 2 indicate that the proposed three-phase CPE homogenization model can be successfully used to describe the experimental data for effective conductivity for PEO-NaI/Al_2O_3 [23] and PEO-$LiClO_4$/PAAM [26] composite systems. The results shown in Fig. 2 were obtained with effective percolation thresholds $g_e^{(1)}$ and $g_e^{(2)}$ of 0.28 and 0.15, respectively [23,32]. The effective percolation slopes t_1 and t_2 were chosen to match the experimental data. In general, the higher the difference in conductivities of the matrix and dispersed phase, the higher the percolation slope. In the present work, it was chosen $t_i = 1$ to minimize the amount of variables involved in calculations and based on the assumption that the particulate phase is conductive in the composites considered here. The results shown in Fig. 2 indicate that GEMT, which uses experimentally determined percolation thresholds, is able to simulate closely the variation of the CPE conductivity as a function of the filler content.

Table 2
EMT models for effective conductivity of a composite material.

McLachlan Generalized Effective Medium Theory (GEMT)	$g\frac{\sigma_f^{1/t} - (\sigma_{eff})^{1/t}}{\sigma_f^{1/t} + [1/g_e - 1](\sigma_{eff})^{1/t}} + (1-g)\frac{\sigma_m^{1/t} - (\sigma_{eff})^{1/t}}{\sigma_m^{1/t} + [1/g_e - 1](\sigma_{eff})^{1/t}} = 0$
Maxwell-Wagner Theory (MWT)	$\frac{\sigma_{eff} - \sigma_f}{\sigma_{eff} + (d-1)\sigma_f} = (1-g)\frac{\sigma_m - \sigma_f}{\sigma_m + (d-1)\sigma_f}$
Asymmetric Bruggeman Effective Medium Theory (ABEM)	$\frac{(\sigma_m - \sigma_{eff})^d}{\sigma_{eff}} = \frac{g^d(\sigma_m - \sigma_f)^d}{\sigma_f}$
Symmetric Bruggeman Effective Medium Theory (SBEM)	$g\frac{\sigma_f - \sigma_{eff}}{\sigma_f + (d-1)\sigma_{eff}} + (1-g)\frac{\sigma_m - \sigma_{eff}}{\sigma_m + (d-1)\sigma_{eff}} = 0$
Series Brick-Layer Model (SBLM)	$\frac{1}{\sigma_{eff}} = \frac{g}{\sigma_f} + \frac{1-g}{\sigma_m}$
Parallel Brick-Layer Model (PBLM)	$\sigma_{eff} = g\sigma_f + (1-g)\sigma_m$
Landau–Lifshitz (LL)	$(\sigma_{eff})^{1/3} = g(\sigma_f)^{1/3} + (1-g)(\sigma_m)^{1/3}$
Hamilton–Crosser (HC)	$\frac{\sigma_{eff} - \sigma_m}{\sigma_{eff} + (n-1)\sigma_m} = g\frac{\sigma_f - \sigma_m}{\sigma_f + (n-1)\sigma_m}$

σ_{eff} – effective composite conductivity; g – reinforcement volume fraction; g_e – effective percolation threshold; t – effective percolation slope; d – system dimensionality; n – inclusion shape factor.

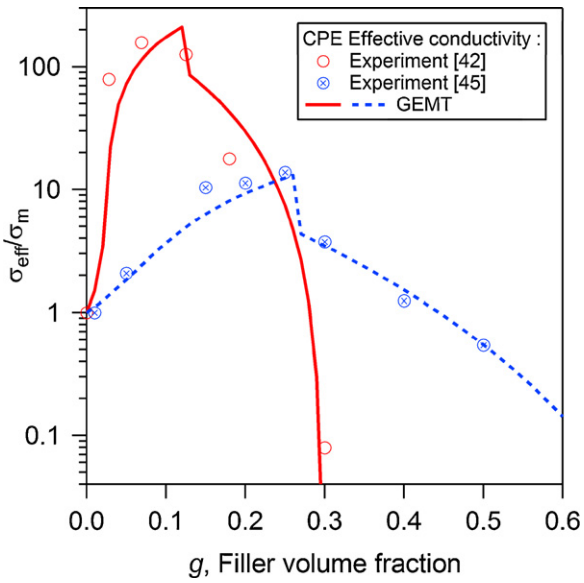

Fig. 2. Experimental and computed dimensionless effective conductivity using GEMT model (data at room temperature).

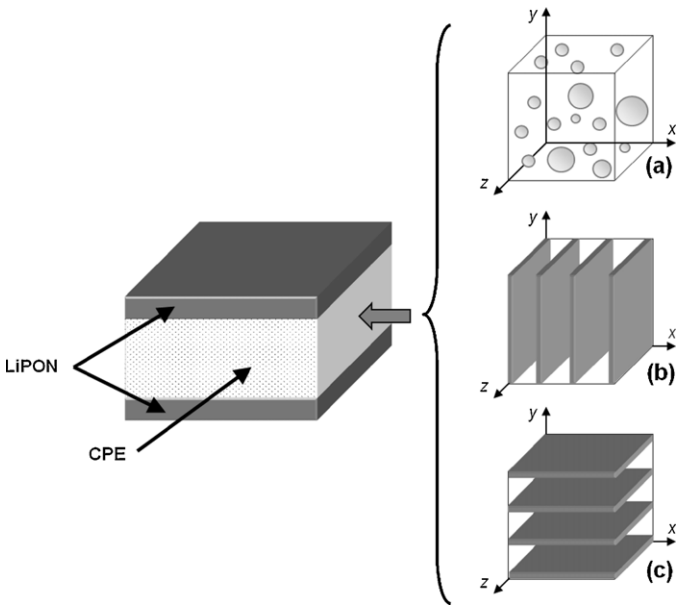

Fig. 3. Proposed solid electrolyte block configuration with different core reinforcement geometries: (a) particulate; (b) vertical layers and (c) horizontal layers.

3.2. Effective elastic constants

Effective stiffness tensor was obtained based on the Mori–Tanaka approach [35–38]. Unlike other homogenization methods, the Mori–Tanaka scheme is applicable to the composites with high volume fractions of the reinforcing phase since it introduces interactions between the filler particles, or inclusions, in the algebraic formulations for the effective stiffness tensor. In this section, this method is briefly described and analytical expressions are given for the case when spherical particles are embedded in the polymer matrix.

The reinforcement inclusions in the composite material are treated as inhomogeneities. The main concept in the Mori–Tanaka approach is that the average strain in inhomogeneities equals that of a single inhomogeneity embedded in a matrix subjected to a uniform matrix strain. Let $\underline{\underline{L}}^{(i)}$ denote the stiffness tensor of the ith phase of the composite material and $\underline{\underline{L}}^{*}$ denote the effective stiffness tensor of the composite. Assuming pure elasticity in each phase $\underline{\sigma}^{(i)} = \underline{\underline{L}}^{(i)}\underline{e}^{(i)}$, the effective elastic behavior of the composite material is described as $\underline{\sigma} = \underline{\underline{L}}^{*}\underline{e}$, with $\underline{\sigma}^{(i)}$, $\underline{e}^{(i)}$ being stress and strain in the phase i and $\underline{\sigma}$, $\underline{e}$ being the overall macroscopic stress and strain tensors correspondingly. By the average theorem [35]

$$\underline{e} = \sum g_i \underline{e}^{(i)} \tag{6}$$

the expression connecting stiffness tensors of the individual phases with the effective stiffness tensor of the composite material can be obtained, as:

$$\sum_i g_i(\underline{\underline{L}}^{(i)} - \underline{\underline{L}}^{*})\underline{e}^{(i)} = 0 \tag{7}$$

If there is a transformation law which connects average strain in inhomogeneity to the average strain of the host material (matrix) ($\underline{e}^{(h)}$) in form $\underline{e}^{(i)} = \underline{\underline{T}}^{(hi)}\underline{e}^{(h)}$, then Eq. (7) can be transformed into the following form

$$\underline{\underline{L}}^{*} = \underline{\underline{L}}^{(h)} + \left[\sum_i g_i(\underline{\underline{L}}^{(i)} - \underline{\underline{L}}^{(h)})\underline{\underline{T}}^{(hi)}\right]\left(g_h\underline{\underline{I}} + \sum_{i\neq h} g_i\underline{\underline{T}}^{(hi)}\right)^{-1} \tag{8}$$

where $\underline{\underline{L}}^{(h)}$ is the stiffness tensor of the host material and $\underline{\underline{I}}$ is the identity tensor. Expression in Eq. (8) represents the Mori–Tanaka model and explicitly gives the result for the effective stiffness tensor of the multi-phase composite material. The effective moduli produced by Mori–Tanaka approach always satisfy Hashin–Shtrikman bounds for two-phase composites [37]. An expression for the transformation tensor $\underline{\underline{T}}$ can be found based on the solution to the problem of an inclusion embedded into matrix as:

$$\underline{\underline{T}}^{(hi)} = [\underline{\underline{I}} - \underline{\underline{S}}^{(i)}(\underline{\underline{L}}^{(h)})^{-1}(\underline{\underline{L}}^{(h)} - \underline{\underline{L}}^{(i)})]^{-1} \tag{9}$$

where $\underline{\underline{S}}^{(i)}$ is the Eshelby tensor derived for the inclusion i. The Eshelby tensor is a function of the inclusion geometry and matrix properties. More detailed information on the derivation of Eshelby tensors can be found in Desrumaux et al. [36]. The components of the Eshelby tensor for spherical inclusions are represented as

$$\begin{aligned} S_{1122} &= S_{2233} = S_{1133} = S_{2211} = S_{3311} = S_{3322} = \frac{5\nu - 1}{15(1-\nu)} \\ S_{1212} &= S_{2323} = S_{3131} = \frac{4 - 5\nu}{15(1-\nu)} \\ S_{1111} &= S_{2222} = S_{3333} = \frac{7 - 5\nu}{15(1-\nu)} \end{aligned} \tag{10}$$

It has to be mentioned that in the present analysis the effect of the amorphous shell surrounding the filler components, on the CPE elastic properties is neglected due to its very low stiffness as compared to that of the filler, effectively resulting in a two-phase composite material. The advantage of the Mori–Tanaka scheme is that it provides an explicit formulation for the effective stiffness tensor.

4. Results and discussion

Three geometrical configurations that are typical for composite materials are evaluated for both effective conductivity and mechanical strength using the methods described in the previous sections. A three-dimensional design of the CPE is considered for this purpose. The envisioned sandwich structure for the CPE between cathode and anode is shown in Fig. 3. Two layers of LiPON should provide stability at the cathode and prevent roughening at the lithium anode. Between them, a composite structure is placed, which consists of a mixture of PEO-based electrolyte,

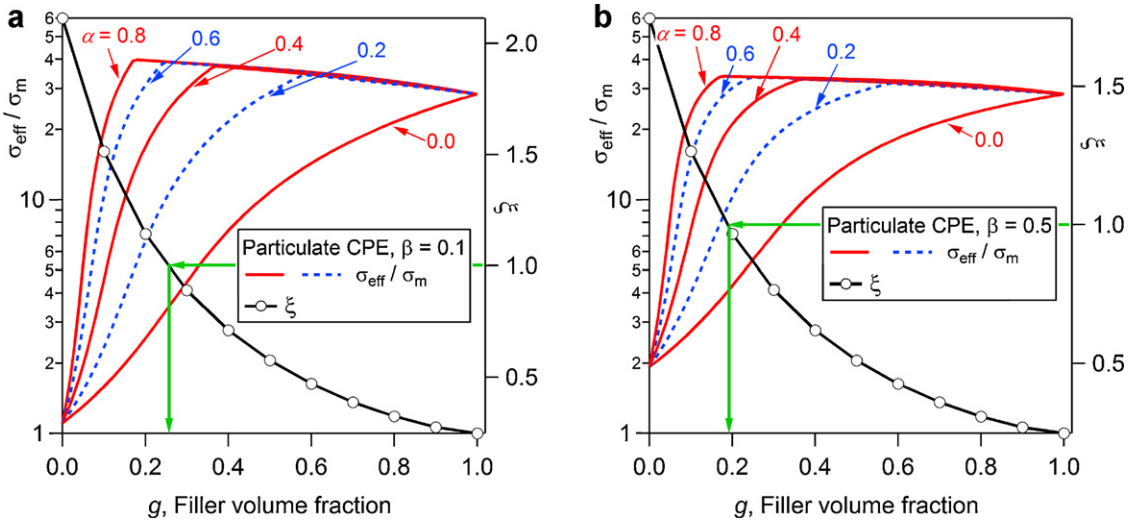

Fig. 4. Effective particulate CPE conductivity and mechanical stability parameter as function of filler volume fraction for different values of parameters α: (a) $\beta = 0.1$ and (b) $\beta = 0.5$.

$(PEO)_{10}LiClO_4$, and LiPON reinforcement inclusions of different geometries, as shown in Fig. 3. From the computational viewpoint, the effective properties of the composite middle layer are computed first and then combined with the two LiPON sheets to give the overall property for the structure. Reuss and Voight limiting approximations were used to obtain effective properties of layered structures [33]. The effective conductivity is computed for y-direction only since this is the direction of interest in battery operation. Therefore, in the subsequent sections σ_{eff} refers to effective conductivity along the y-axis.

The results are organized such that the effective conductivity and mechanical properties can be shown side-by-side as a function of the LiPON amount in the overall CPE. For the conductivity results, the conductivities of the individual phases were those shown in Table 2. Unless otherwise specified, the Young's modulus for the PEO is considered to be 5 GPa, which was measured for thin-films [30], due to the thin-film nature of the solid electrolytes. The estimated properties are reported in dimensionless form. The parameter β represents the ratio of the thickness of the two LiPON sheets over the total thickness of the composite electrolyte block. The effective conductivity is normalized with respect to the conductivity of the polymer matrix and the effective shear modulus of the electrolyte block is normalized with respect to the shear modulus of the lithium metal. Effective conductivity is shown for five different values of the relative shell thickness α. Cases without the conductive shell were represented by $\alpha = 0$. Since it was assumed in this study that the thickness of the conductive amorphous shell is constant, when present, and does not depend on the particle size, different values of α represent in fact the different particle sizes.

The computed results of the effective properties for electrolyte blocks with a particulate CPE core (Fig. 3a) are represented in Fig. 4. The results are reported here for $\beta = 0.1$ (Fig. 4a) and 0.5 (Fig. 4b). The following observations can be made based on the results in Fig. 4. The polymer matrix is the least conductive phase and the addition of the LiPON filler increases the conductivity of the CPE. Such increase obviously happens even in the case when the amorphous layer is absent ($\alpha = 0$). In the presence of the conductive shell, the increase in the effective conductivity is followed by a slight decrease, corresponding to the saturated state when the particles come into contact with each other. Since the conductivity of LiPON is rather close to the conductivity of the amorphous PEO, such a decrease is not as dramatic as the one observed in mixtures of

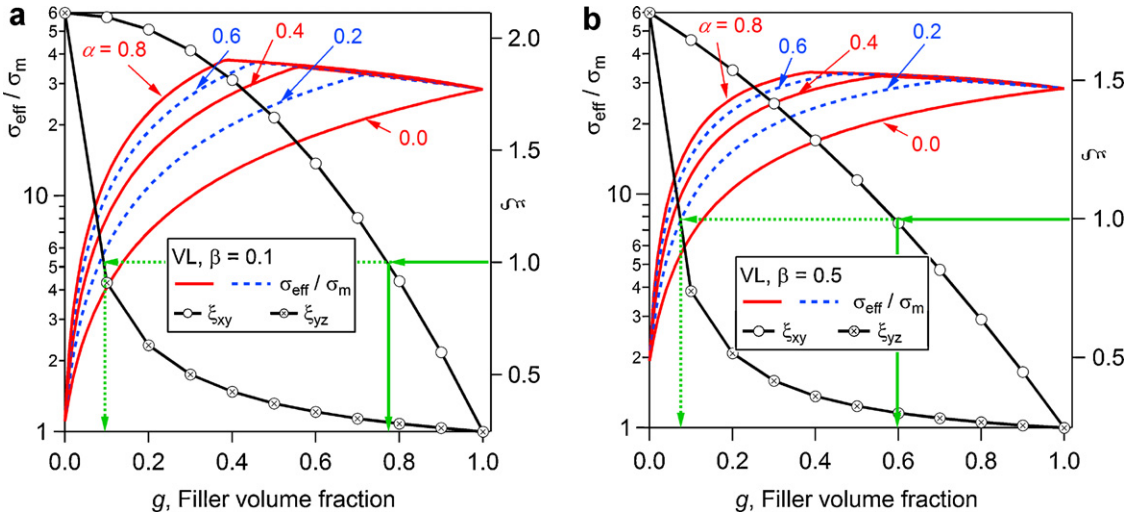

Fig. 5. Effective conductivity and mechanical stability parameter of vertically layered composite electrolyte as function of filler volume fraction for different values of parameters α: (a) $\beta = 0.1$ and (b) $\beta = 0.5$.

non-conductive ceramics with polymer electrolytes [23]. The rate of the initial increase of the effective conductivity with respect to the filler volumetric fraction seems to be proportional to the value of parameter α; i.e., the maximum conductivity is achieved at lower volumetric fractions for larger values of α. After the initial increase, the curves corresponding to different values of parameter α merge together and decrease to the value characteristic of conductivity of the filler phase. Such a behavior is observed in both cases of parameter β. In case of thicker ($\beta = 0.5$) LiPON boundary sheets, however, the maximum conductivity achieved is lower than in the case when the LiPON sheet thickness is 0.05 times the total thickness of the composite block ($\beta = 0.1$). The highest enhancement in conductivity is found to be approximately 40 times the conductivity of PEO matrix. The arrows in Fig. 4 demarcate the region where the stability parameter ξ attains the value of 1.0. It can be seen that such an enhancement in mechanical properties can be achieved within reasonably low (below random close packing limit of 0.64 [39,40]) volume fractions of LiPON: $g = 0.26$ for the case of $\beta = 0.1$ and $g = 0.19$ for the case of $\beta = 0.5$. Obviously, with thicker LiPON sheets sandwiching the CPE, this criteria would be met at the lower volume fractions of particulate loading. However, the difference between the threshold volume fractions corresponding to $\beta = 0.1$ and $\beta = 0.5$ is rather small, since, with the increase of the LiPON sheet thickness comes a trade-off in terms of higher Young's modulus and lower values of Poisson's ratio for the composite electrolyte block, which results in higher value of ξ.

Another aspect that needs to be investigated is the gain (or loss) in the effective conductivity at the levels of the LiPON volume fractions where the mechanical stability criterion is met. When $\alpha = 0.0$ the gain in effective conductivity is slightly higher for thicker bounding LiPON sheets ($\sigma_{eff}/\sigma_m = 4.1$ for $\beta = 0.5$ and $\sigma_{eff}/\sigma_m = 3.4$ for $\beta = 0.1$). In all other cases ($\alpha \neq 0.0$) the effective conductivity is higher when thin bounding layers of LiPON are used. This becomes especially pronounced at high values of parameter α ($\sigma_{eff}/\sigma_m = 29$ for $\beta = 0.5$ and $\sigma_{eff}/\sigma_m = 39$ for $\beta = 0.1$ when $\alpha = 0.6$). Based on the above considerations it can be stated that rather thin layers of LiPON would provide mechanical properties of the composite electrolyte block that meet the Li stability criteria at reasonable volume fractions of particulate reinforcement without sacrificing the conductivity enhancement.

The results for the vertically layered (VL) CPE (Fig. 3(b)) sandwiched between the horizontal LiPON sheets are shown in Fig. 5. In the case of layered structures, the parameter α represents the ratio

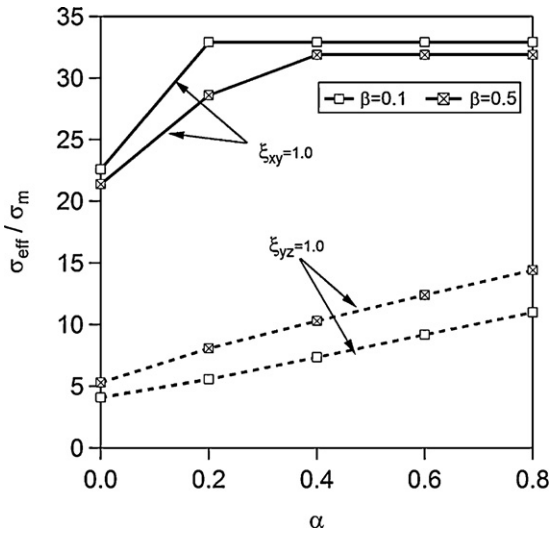

Fig. 6. Normalized effective conductivity as a function of dimensionless shell thickness parameter α for VL composite electrolyte.

of the shell thickness over the thickness of the reinforcing layer. Due to the directional reinforcement of the CPE by LiPON layers, the material properties cannot be considered symmetric with respect to rotation about y-axis and therefore two values of shear modulus (G_{xy} and G_{yz}) and two values of Poisson's ratio (ν_{xy} and ν_{yz}) are considered. This correspondingly results in two values of the stability parameter: ξ_{xy} and ξ_{yz}. The electrode stability criteria are applied to both values. It can be seen from Fig. 5 that while the $\xi_{yz} = 1.0$ criterion is met at low volume fraction of LiPON layers, the same criteria for ξ_{xy} is satisfied at rather high content of reinforcement (~80% and ~60% for $\beta = 0.1$ and 0.5 respectively). It should be mentioned that such high volume fractions are practically achievable in case of layered composites. Obviously, the stability parameter corresponding to the stiffer direction yz does not change significantly with increase of the thickness of boundary LiPON layers.

Behavior of effective conductivity at reinforcement volume fractions when the $\xi = 1.0$ stability criterion is met is shown in Fig. 6. The normalized effective conductivity is shown as a function of conductive shell thickness parameter α for two values of parameter β. This way the effect of increasing the thickness of boundary LiPON

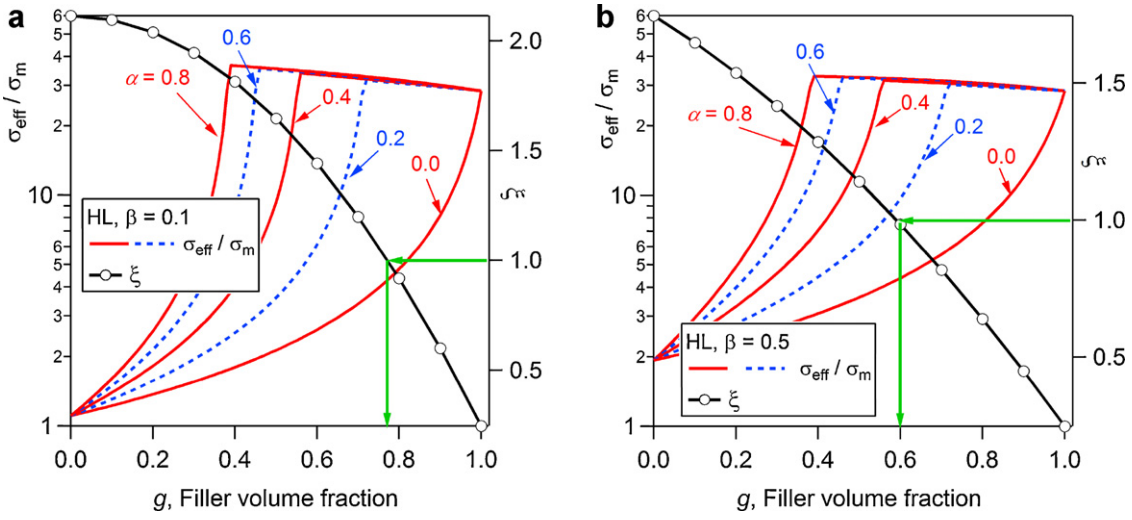

Fig. 7. Effective conductivity and mechanical properties of horizontally layered composite electrolyte as function of filler volume fraction for different values of parameters α: (a) $\beta = 0.1$ and (b) $\beta = 0.5$.

layers on effective conductivity can be estimated. Because the $\xi_{xy} = 1.0$ condition is met at higher volume fractions, the effective conductivity does not change significantly with increase in both α and β. At the same time the normalized effective conductivity increases by about factor of 1.5 at high values of α when thicker boundary sheets are used (Fig. 6). It should be mentioned that in order to suppress amplification of electrode surface roughness, the stability criterion should be met in both directions for such transversely isotropic material and therefore the composite is expected to be fabricated with high volume concentration of LiPON layers. The results for the horizontally layered (HL) CPE (Fig. 3(c)) are shown in Fig. 7. The mechanical properties are symmetric with respect to rotation about y-axis and therefore $G_{xy} = G_{yz} = G_{eff}$ and $\nu_{xy} = \nu_{yz} = \nu_{eff}$. One stability criterion $\xi = 1.0$ thus is used. It can be seen from Fig. 7 that high content of LiPON is needed to maintain stability of the electrode surface when horizontally layered composite electrolyte is used. However, such high concentrations are technically achievable and provide rather good enhancement in effective conductivity when amorphous conductive shell is absent ($\alpha = 0$).

Analysis of the results shown in Figs. 4–7 for three different large-scale reinforcement geometries reveals the interplay of different effective properties that make a composite electrolyte block suitable for battery applications when the lithium metal anode is employed. The configuration suggested here, with the placement of CPE between two LiPON layers, was sought to improve the stiffness of electrolyte and further prevent the anode roughening and dendrite formation. For some configurations, the analysis is more complicated as more variables had to be considered and two stability criteria must be satisfied. In some cases, the sandwich CPE may reduce the benefit of improved conductivity of the electrolyte. The higher values of shear modulus are achieved by either increasing the thickness of boundary LiPON layers or by increasing the reinforcement content in the middle CPE section. In both cases this results in lower values of Poisson's ratio. The combined influence of the shear modulus and Poisson's ratio on the stability of the electrode surface can be assessed by the stability parameter ξ (Eq. (1)) which was deduced from the reported results of effect of mechanical properties of electrolyte on amplification of electrode roughness [1].

Figs. 4–7 demonstrate that the stability criteria can be satisfied in all of the three cases of reinforcement geometry inside the CPE layer. The lowest reinforcement volume fraction, which allows for $\xi = 1.0$, is found in CPE with particulate reinforcement and LiPON sheet thickness of 25% of the total thickness of the electrolyte (Fig. 4b). It should be re-iterated here that the existence of amorphous polymer interfacial layer has not been experimentally confirmed for LiPON/PEO systems. Therefore the results for $\alpha \neq 0$ are presented for comparison purposes and the discussion should be mainly based on the behavior of mixture of bare LiPON with PEO electrolyte. From this perspective, the highest conductivity at point when $\xi = 1.0$ is achieved in vertically layered electrolyte blocks, with the conductivity being improved by 22 times as compared to polymer matrix conductivity (Fig. 6). This improvement is achieved at rather large content of LiPON layers (~80%). However the benefit of conductivity improvement could make this arrangement the most promising. The 20% of the volume in this case would be occupied by the polymer, which may improve the ductility of the electrolyte and prevent it from cracking.

For the sake of completeness, results for the stability threshold parameter are now presented for other values of the Young's modulus of the polymer. Fig. 8 shows the effect of polymer elastic

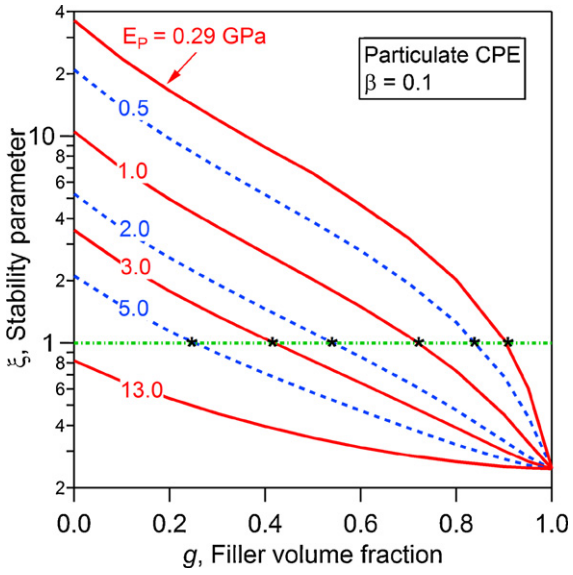

Fig. 8. Effect of the polymer Young's modulus (E_P) on the stability parameter for particulate CPE.

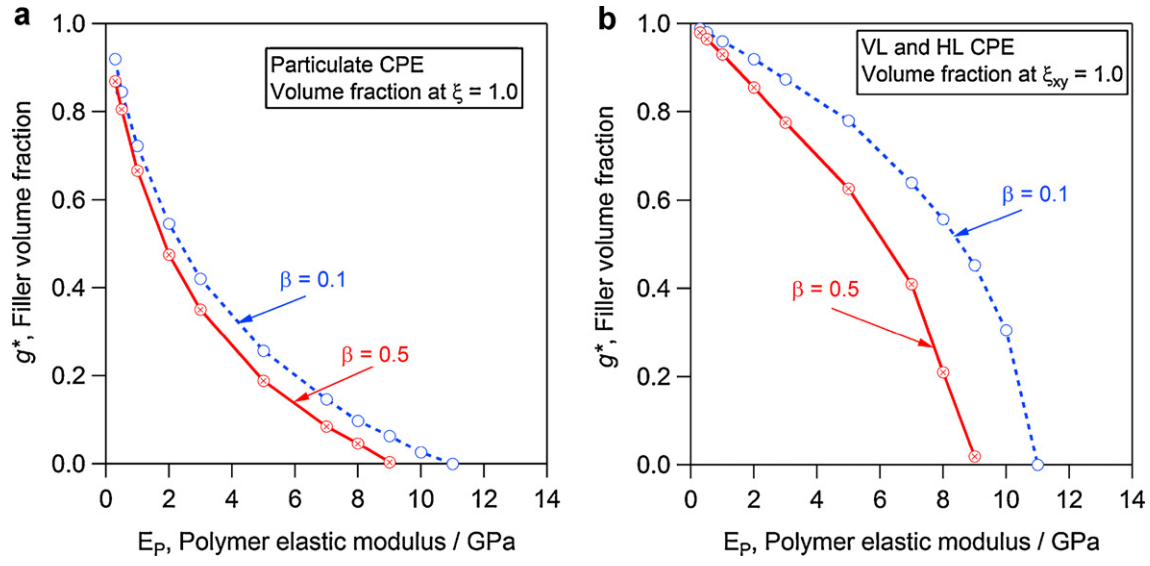

Fig. 9. Amount of reinforcement required to achieve mechanical stability of CPE as a function of polymer Young's modulus: (a) particulate CPE and (b) VL and HL CPE.

modulus (E_P) on the behavior of stability parameter for the case of particulate CPE. The values of the modulus range from 0.29 GPa to the chain limit of 13 GPa determined from Raman measurements [31]. The points where stability criterion is satisfied are marked with asterisks. Apparently rather high loadings of filler are required to achieve stability as the modulus approaches its lower limit.

The volume fractions (g^*) corresponding to $\xi = 1.0$ are plotted against the Young's modulus of the polymer in Fig. 9. Since the HL composite represents the 90° rotation of the VL composite about z-axis, which is the axis of symmetry for transversely isotropic material, the values of ξ in xy plane coincide for both VL and HL cases and are represented in one plot (Fig. 9b). Interestingly, the effect of increase in boundary reinforcement sheets is not pronounced for the case of particulate CPE (Fig. 9a). It can be seen from Fig. 9 that no reinforcement is necessary to achieve the stability when the polymer elastic modulus reaches values of 9 GPa and 11 GPa for $\beta = 0.5$ and 0.1 respectively. These values are rather high even for the most stiff block co-polymers synthesized nowadays for Li ion battery electrolyte [41,42]. Therefore, it can be stated that fabrication of composite systems is necessary in order to suppress electrode roughening. Particle reinforced isotropic composites seem to be the best choice to achieve the stability with lower amount of stiffening phase. The results reported in this study can be used as guidelines for CPE design. Finally, the choice of geometrical configurations for CPE electrolytes would also depend on the manufacturing requirements to produce such an arrangement with minimal cost.

5. Conclusions

The data presented in this study for three different large-scale reinforcement geometries reveals the interplay among several effective properties that make a composite electrolyte block suitable for battery applications when the lithium metal anode is employed. A homogenization model for a three-phase media was used to evaluate the effective CPE conductivity. Effective stiffness tensor, from which the shear modulus and Poisson's ratio were estimated, was obtained based on the Mori–Tanaka approach. The dependence of effective conductivity and electrode mechanical stability parameter on such variables as filler volume fraction, thickness of highly conductive interfacial layer, and polymer elastic modulus has been studied. Both elastic and compressible properties, through shear modulus and Poisson's ratio, are considered to formulate a mechanical stability criterion. In order to increase the resistance to electrode roughening, the proposed electrolyte structure consisted of CPE (either particulate or layered) block sandwiched between two horizontal layers of LiPON. The results indicate that the lowest volume fraction of reinforcement capable of making electrolyte suitable for dendrite suppression can be achieved with particulate CPE. At the same time the best conductivity would be achieved in vertically layered structures at high reinforcement content.

Acknowledgements

This research was sponsored by the Laboratory Directed Research and Development Program of Oak Ridge National Laboratory (ORNL), managed by UT-Battelle, LLC for the U. S. Department of Energy under Contract No. DE-AC05-00OR22725.

References

[1] C. Monroe, J. Newman, J. Electrochem. Soc. 152 (2) (2005) A396–A404.
[2] J.B. Bates, N.J. Dudney, G.R. Gruzalski, B.A. Zuhr, A. Choudhury, C.F. Luck, J.D. Robertson, Solid State Ionics 53–56 (1992) 647–654.
[3] X. Yu, J.B. Bates, G.E. Jellison Jr., F.X. Hart, J. Electrochem. Soc. 144 (2) (1997) 524–532.
[4] J.B. Bates, N.J. Dudney, B. Neudecker, A. Ueda, C.D. Evans, Solid State Ionics 135 (2000) 33–45.
[5] N.J. Dudney, G.-A. Nazri, G. Pistoia (Eds.), Lithium Batteries: Science and Technology, Kluwer Publishing Company, Norwell, MA, 2004, pp. 623–642.
[6] F. Croce, B. Scrosati, G. Mariotto, Chem. Mater. 4 (1992) 1134–1136.
[7] F. Croce, G.B. Appetecchi, L. Persi, B. Scrosati, Nature 394 (1998) 456–458.
[8] B. Scrosati, F. Croce, S. Panero, J. Power Sources 100 (2001) 93–100.
[9] F. Croce, S. Sacchetti, B. Scrosati, J. Power Sources 161 (2006) 560–564.
[10] J.E. Weston, B.C.H. Steele, Solid State Ionics 7 (1982) 75–79.
[11] J. Przyluski, W. Wieczorek, Solid State Ionics 36 (1989) 165–169.
[12] M.A.K.L. Dissanayake, P.A.R.D. Jaythilaka, R.S.P. Bokalawala, I. Albinsson, B.E. Mellander, J. Power Sources 119–121 (2003) 409–414.
[13] H.M.J.C. Pitawala, M.A.K.L. Dissanayake, V.A. Senevirante, Solid State Ionics 178 (2007) 885–888.
[14] G.B. Appetecchi, F. Croce, G. Dautzenberg, M. Mastragostino, F. Ronci, B. Scrocati, F. Soavi, A. Zanelli, F. Alessandrini, P.P. Prosini, J. Electrochem. Soc. 145 (12) (1998) 4126–4132.
[15] J. Syzdek, M. Armand, M. Marcinek, A. Zalewska, G. Zukowska, W. Wieczorek, Electrochim. Acta 55 (2010) 1314–1322.
[16] M. Egashira, Y. Utsunomiya, N. Yoshimoto, M. Morita, Electrochim. Acta 52 (2006) 1082–1086.
[17] A. Bac, M. Ciosek, M. Bukat, M. Marczewski, H. Marczewska, W. Wieczorek, J. Power Sources 159 (2006) 405–411.
[18] C.Y. Pan, Q. Feng, L.J. Wang, Q. Zhang, M. Chao, J. Central South Univ. Technol. 3 (2007) 348–352.
[19] M. Siekierski, P. Rzeszotarski, K. Nadara, Solid State Ionics 176 (2005) 2129–2136.
[20] J. Przyluski, M. Siekierski, W. Wieczorek, Electrochim. Acta 40 (1995) 2101–2108.
[21] W. Wieczorek, A. Zalewska, M. Siekerski, J. Przyluski, Solid State Ionics 86–88 (1996) 357–362.
[22] C.W. Nan, D.M. Smith, Mater. Sci. Eng. B10 (1991) 99–106.
[23] W. Wieczorek, M. Siekierski, J. Appl. Phys. 76 (4) (1994) 2220–2226.
[24] W. Wieczorek, A. Zalewska, D. Raducha, Z. Florjanczyk, J.R. Stevens, Macromolecules 29 (1996) 143–155.
[25] A. Zalewska, W. Wieczorek, J.R. Stevens, J. Phys. Chem. 100 (1996) 11382–11388.
[26] W. Wieczorek, K. Such, Z. Florjanczyk, J.R. Stevens, J. Phys. Chem. 98 (1994) 6840–6850.
[27] E.G. Herbert, W.E. Tenhaeff, N.J. Dudney, G.M. Pharr, Thin Solid Films (2011) doi:10.1016/j.tsf.2011.07.068.
[28] H.Y. Nie, M. Motomatsu, W. Mizutani, H. Tokumoto, J. Vac. Sci. Technol. B13 (1995) 1163–1166.
[29] R.W. Warfield, F.R. Barnet, Die Angew. Makromol. Chem. 27 (410) (1972) 215–217.
[30] L.M. Bellan, J. Kameoka, H.G. Craighead, Nanotechnology 16 (2005) 1095–1099.
[31] K. Song, S. Krimm, J. Polymer. Sci. 28 (1990) 63–69.
[32] D.G. Han, G.M. Choi, Solid State Ionics 106 (1998) 71–87.
[33] M. Wang, N. Pan, Mater. Sci. Eng. R 63 (2008) 1–30.
[34] S. Kalnaus, A.S. Sabau, S. Newman, W.E. Tenhaeff, C. Daniel, N.J. Dudney, Solid State Ionics 199–200 (2011) 44–53.
[35] Z. Hashin, J. Appl. Mech. 50 (1983) 481–505.
[36] F. Desrumaux, F. Meraghni, M.L. Benzeggagh, J. Composite Mater. 35 (2001) 603–624.
[37] J.G. Berryman, P.A. Berge, Mech. Mater. 22 (1996) 149–164.
[38] Y. Benveniste, Mech. Mater. 6 (1987) 147–157.
[39] K.W. Desmond, E.R. Weeks, Phys. Rev. E 80 (2009) 051305–51311.
[40] E.L. Hinrichsen, J. Feder, T. Jøssang, Phys. Rev. A 41 (8) (1990) 4199–4209.
[41] A. Panday, S. Mullin, E.D. Gomez, N. Wanakule, V.L. Chen, A. Hexemer, J. Pople, N.P. Balsara, Macromolecules 42 (2009) 4632– 4637.
[42] M. Singh, O. Odusanya, G.M. Wilmes, H.B. Eitouni, E.D. Gomez, A.J. Patel, V.L. Chen, M.J. Park, P. Fragouli, H. Iatrou, N. Hadjichristidis, D. Cookson, N.P. Balsara, Macromolecules 40 (2007) 4578–4585.